Journal of Nuclear Materials 420 (2012) 497–500

Contents lists available at SciVerse ScienceDirect

Journal of Nuclear Materials

journal homepage: www.elsevier.com/locate/jnucmat

Banded structure and its distribution in friction stir processing of 316L austenitic stainless steel

Y.C. Chen [a,*], H. Fujii [a], T. Tsumura [a], Y. Kitagawa [a], K. Nakata [a], K. Ikeuchi [a], K. Matsubayashi [b], Y. Michishita [b], Y. Fujiya [b], J. Katoh [c]

[a] Joining and Welding Research Institute, Osaka University, Osaka 567-0047, Japan
[b] Manufacturing Technology Center, Mitsubishi Heavy Industries, Ltd., Takasago 676-8686, Japan
[c] Advanced Nuclear Plant Designing Section, Mitsubishi Heavy Industries, Ltd., Kobe 652-8585, Japan

ARTICLE INFO

Article history:
Received 23 February 2009
Accepted 26 October 2011
Available online 11 November 2011

ABSTRACT

Banded structures, which vary with welding parameters, were observed in friction stir processing of 316L austenite stainless steel. Sigma phase precipitation was detected in banded structures by transmission electron microscopy. The amount of banded structure had direct ratio relations with heat input. The higher the heat input, the larger the area of banded structures. This is attributable to slower cooling rate at high heat input, which results in longer exposure to the temperature range for precipitation. The formation of sigma phase produced Cr depletion, which resulted in largely degraded corrosion resistance. The present study suggests that low heat input (i.e. low rotation speeds, low working loads and high welding speed) contributes to restrain sigma phase precipitation.

1. Introduction

Austenitic stainless steels are widely used in components designed for high temperature applications such as boilers, heat exchangers and chemical reactors. AISI type 316 stainless steel and its modified grades like 316L have applications as structural material in nuclear power plants for the construction of water storage tanks. The choice of this alloy is based on its excellent high temperature tensile and creep-fatigue strengths in combination with good fracture toughness [1,2]. As nuclear plants around the world grow older there are increasing incidences of stress corrosion cracking (SCC) problems. The repair of SCC is becoming an urgent task to extend the service life of stainless steel water storage tanks which have experienced SCC cracks at the external surface. As a solid state welding technology, Friction stir welding (FSW) [3] can weld low temperature materials such as Al alloys [4–11] and Mg alloys [12–16] and gets high quality joints than fusion welding technology. Such good merits are also expected for joining high temperature materials like stainless steel. Some studies have reported the feasibility of FSW of stainless steels [17,18]. Friction stir processing (FSP) is a technique which has grown out of FSW technology and essentially provides a high integrity smooth repair of shallow surface defects. Compared with conventional weld repair methods, this technology can offer advantages for on-line application particularly in terms of its lower risk of through-wall penetration.

Sigma phase precipitation was first observed in FSW of 304 austenite stainless steel by Park et al. [17,18]. They reported that small amount of sigma phases were rapidly formed along the grain boundaries in the advancing side of the stir zone in banded structures [17,18]. In general, the presence of sigma phase will not only affect mechanical properties of the material, but also reduce its corrosion resistance [19]. Therefore, it is important to determine what factor affects the precipitation of sigma phase. Despite the need for a general understanding of the sigma phase precipitation, most investigations carried out to date are only focus on the observations of sigma phase precipitation in specific materials. In current experiments, the formation of banded structures in stir zone is also detected in FSP of 316L austenite stainless steel. The objective of the present study is to investigate the key factor of the formation of banded structures and its distribution.

2. Experimental

The base metal is a 15-mm-thick 316L stainless steel plate. The chemical compositions and mechanical properties of the base metal are shown in Table 1. Rectangular welding samples, 250 mm long by 200 mm wide, are processed using a FSW machine. FSP experiments are carried out by bead-on-plate method. After a series of feasibility tests, following experimental parameters are selected in this study. The processing parameters are rotation speeds of 4, 5 and 6 rad s^{-1} and welding speeds of 16, 20 and 24 mm min^{-1}. The working loads of the tool are 25, 30 and 35 kN. The tool is fabricated from polycrystalline cubic boron nitride (PCBN) and consists of a convex shoulder having a diameter of 22 mm and a tapered pin.

* Corresponding author. Tel.: +44 161 306 8847.
E-mail address: armstrong@hit.edu.cn (Y.C. Chen).

0022-3115/$ - see front matter © 2011 Elsevier B.V. All rights reserved.
doi:10.1016/j.jnucmat.2011.10.053

Table 1
Chemical compositions and mechanical properties of BM.

BM	Chemical compositions (mass%)									Mechanical properties	
	C	Si	Mn	P	S	Ni	Cr	Mo	Fe	Strength (MPa)	Elongation (%)
316L steel	0.014	0.6	1.2	0.03	0.002	12.1	17.3	2.1	Bal.	545	64

The pin tapers from 9 mm at the shoulder to 4 mm at the pin tip. The shoulder surface has a spiral pattern to enhance the stirring effect. The length of the pin is 5 mm and the welding tilt angle is 0 degree. To avoid surface oxidation, argon shielding is employed around the tool during FSP.

After FSP, the FSP zone is cross-sectioned perpendicular to the welding direction for the metallographic analyses using an electrical-discharge cutting machine. Microstructural observations are performed by optical microscopy (OM), transmission electron microscopy (TEM) and ERA-8800FE scanning electron microscopy (SEM) equipped with an energy-dispersive X-ray spectroscopy (EDS) analysis system. The specimens for OM and SEM are mechanically ground with water abrasive paper and polished with 3 and 1 μm diamond, and etched electrolytically in a solution of 10% oxalic acid + 90% water with a power supply set to 15 V for 90 s. Thin disks for TEM are cut from the expected locations in the FSP zone using a focused ion beam (FIB) instrument (Hitachi High-Technologies FB-2000A). The thin disks are observed at 200 kV using JEOL JEM-2010 TEM.

3. Results and discussion

A low-magnification overview of the transverse cross-section of a typical FSP zone is shown in Fig. 1. This zone has no internal defects. Three distinct zones can be identified, i.e. the stir zone (SZ), the thermo-mechanically affected zone (TMAZ) and the base metal (BM). SEM micrographs of the BM (position A) and several characteristic positions in the SZ (positions B, C and D) are indicated in Fig. 2. Moreover, banded structures are detected in the SZ as marked in Fig. 1. The microstructure in banded structure zone is characterized using TEM and the results are shown in Fig. 3.

It can be seen from Fig. 2a that the BM has an annealed coarse grain structure ranging in size from 30 to 80 μm. No significant corrosion pits are observed in the BM after etching. Fig. 2b shows the microstructure in banded structure area. Linear structure distributes in the banded area. It is serious of etch pits. Fig. 2c shows the SEM micrograph of un-banded structure in the center of the SZ. The grains in the SZ are refined by the tool. The SZ shows a roughly equiaxed grain structure and the grain size is in range of 10–30 μm. No etch pits are found in this region. It means that this region is insensitive to etching. Fig. 2d shows the microstructure at the bottom of the SZ. Similar lamellar structures are found in the bottom of the SZ. Alternate bands of the region are sensitive to etching. SEM images indicate that the corrosion resistance of un-banded structure region in the SZ is similar to that of the BM, but the corrosion resistance of banded structure region is largely degraded.

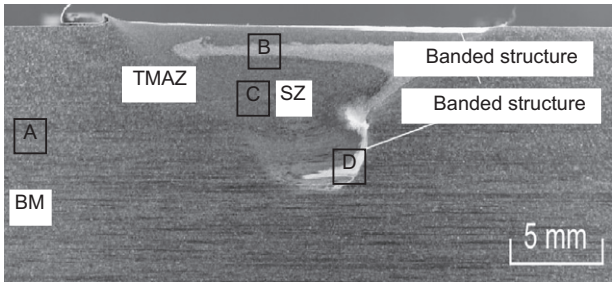

Fig. 1. Low-magnification overview of transversal cross-section of a typical friction stir welding zone (30 kN, 5 rad s^{-1}, 20 mm min^{-1}) [24].

TEM image (Fig. 3a) indicates that the regions with banded structure have short rod-like particles with size of 200–300 nm both along the grain boundaries and in the grain interiors. EDS spectra obtained from positions 1–4 are analyzed in this study. The particle in position 2 consists of 73 wt% Cr, 26.1 wt% Fe and 0.65 wt% Ni, while the region in position 3 consists of 29.3 wt% Cr, 51.5 wt% Fe and 17.2 wt% Ni. The chemical compositions of the particles in positions 1 and 4 are similar to that in position 2. EDS results suggest that the particles should be Cr-rich carbides or sigma phases. The electron diffraction pattern obtained from the particle 2 is shown in Fig. 3b. The electron diffraction pattern reveals that the particle is sigma phase with tetragonal structure.

Moreover, from EDS results we can know that the content of Cr in the sigma phase is higher than that around the precipitates. This result suggests that the formation of Cr-rich sigma phase in this region results in Cr depletion around them. This would be a reason for the reduction of the corrosion resistance in the banded structure area in the SZ. The presence of Cr depletion worsens the corrosion resistance of banded area, resulting in serious of etch pits in banded structure region.

It is well known that the presence of sigma phase will not only reduce the corrosion resistance of the material, but also affect its mechanical properties. Therefore, it is necessary to determine what factor affects the precipitation of sigma phase during FSP.

The real volume fraction of sigma phase in the SZ is difficult to evaluate in current analysis conditions. However, the area of banded structure can indirectly represent the relative volume fraction of sigma phase in the SZ. In this study, the area of banded structure at different processing conditions is measured to qualitatively evaluate sigma phase contents in the SZ. The results are shown in Fig. 4.

The *Y*-axis represents the area with sigma phase precipitation and the *X*-axis represents different processing conditions, i.e. working loads, rotation speeds and welding speeds. Both load control mode and displacement control mode are used for comparisons as shown in Fig. 4. Experimental results show that the area with sigma phase precipitation has direct ratio relations with working loads and rotation speeds and inverse ratio with welding speeds in current experimental conditions. In order to obtain the illustrative diagram of this relationship, the expression of rotation speed multiplying load divided by welding speed is taken as *X*-axis in Fig. 4. For FSP, this expression just approximately represents the heat input tendency in theory. From this figure we can know that the profile of the area with sigma phase precipitation as a function of heat input has a linearity feature in both control modes.

In current processing parameter range, the area with sigma phase precipitation at highest heat input conditions are about three times that at lowest heat input conditions. These results indicate that heat input has a significant effect on the sigma phase precipitation in FSP of 316L stainless steel. The higher the heat input, the larger the area with sigma phase precipitation.

In order to proof the correctness of the relations between heat input and the expression of rotation speed multiplying load divided by welding speed, the peak temperatures in some typical

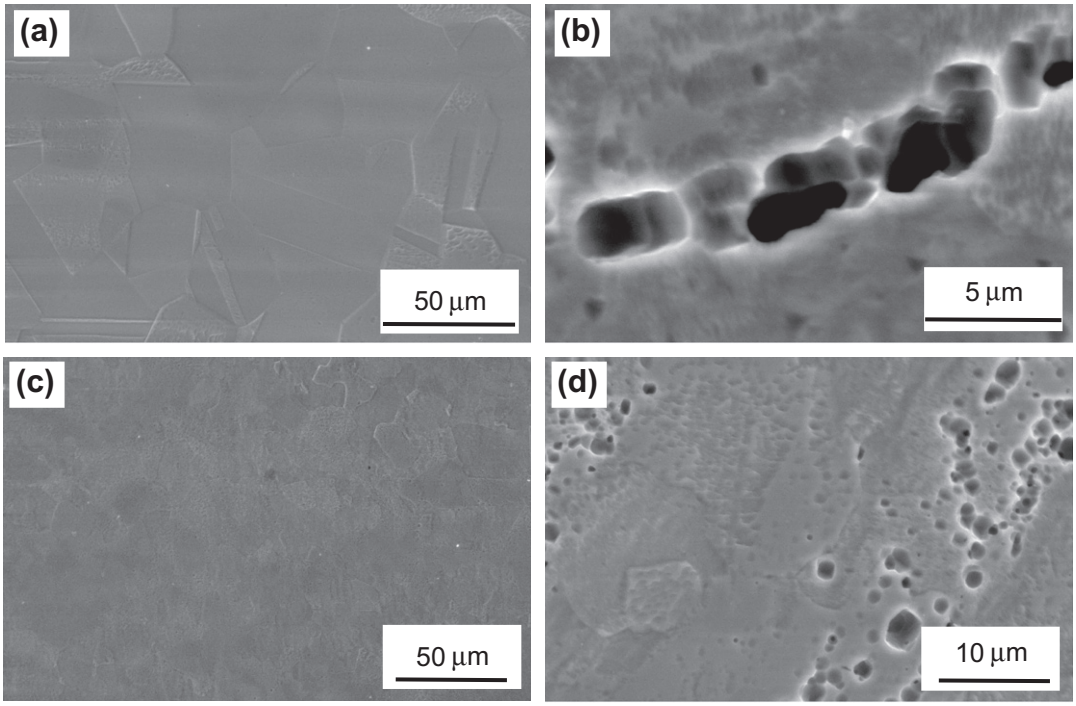

Fig. 2. SEM micrographs of different positions shown in Fig. 1; (a) position A, (b) position B, (c) position C, and (d) position D.

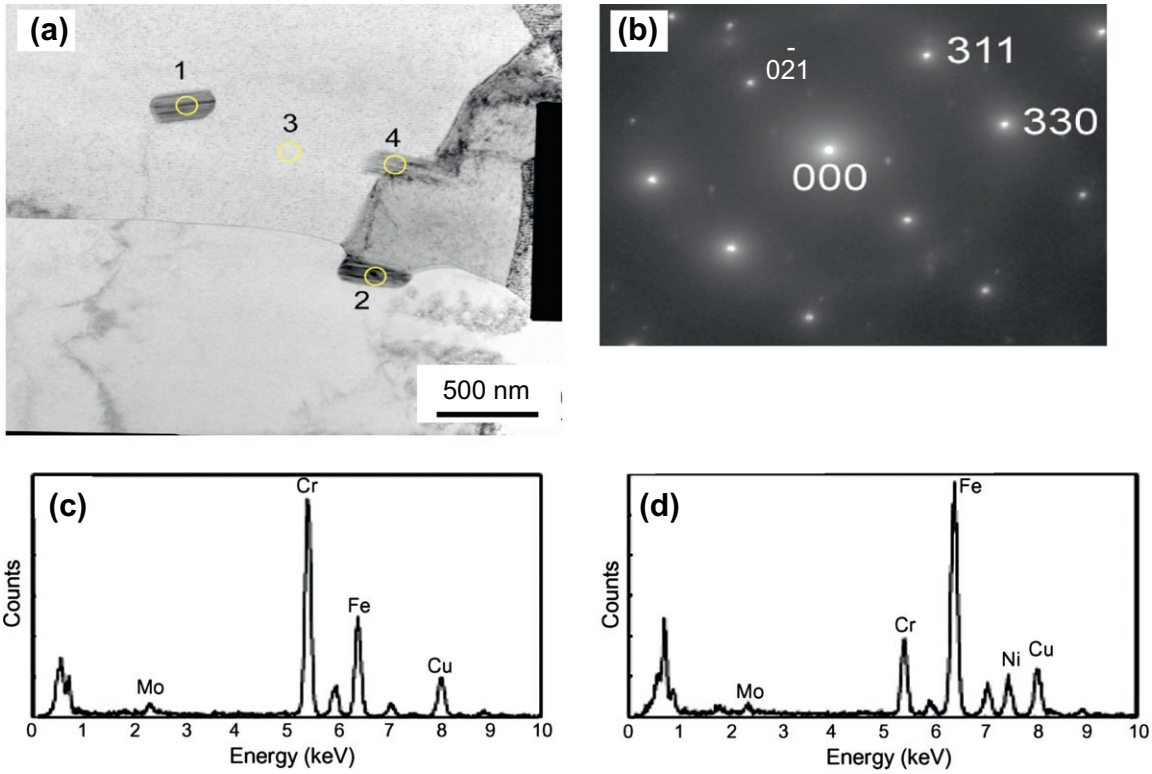

Fig. 3. TEM micrographs of banded structure; (a) bright field image [24], (b) diffraction spot from position 2, (c) EDS analysis from position 2, and (d) EDS analysis from position 3.

parameters ranges were measured during FSP. These parameters ranges, regions A, B and C, are marked in Fig. 4.

The measure position of K-type thermocouples is at the end of PCBN tool. The vertical distance from the end of PCBN tool to the shoulder external diameter is 6.8 mm. Therefore, the peak temperature should be lower than that in the SZ. Although the peak temperature data do not represent the peak temperature in the SZ during FSP, they can reflect the tendency of peak temperature as a function of different processing conditions.

Temperature test results show that the peak temperatures in regions A, B and C shown in Fig. 4 are about 973 K, 1023 K and 1120 K, respectively. It means that the peak temperature in the

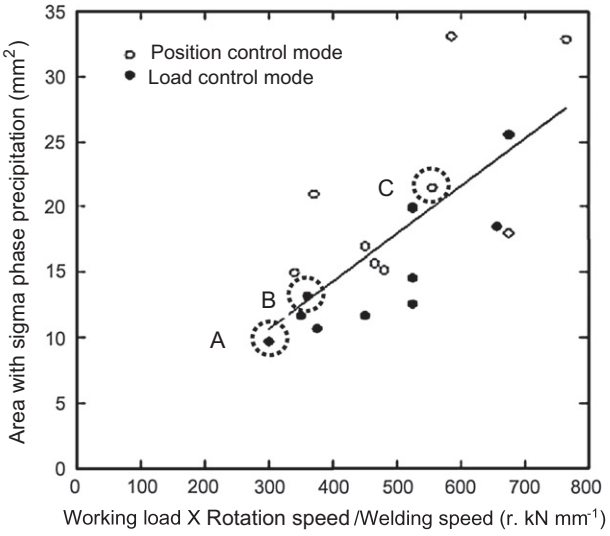

Fig. 4. The area with sigma phase precipitation as a function of heat input in both control modes.

SZ is higher than these values. Okamoto et al. reported that the SZ was exposed to a higher temperature, at least 1473 K during FSW [20]. In addition, temperature test results indicate that the profile of peak temperature as a function of rotation speed multiplying load divided by welding speed shows a linearity feature. These experimental results proof our previous analysis about the identity relations between heat input and this expression.

The formation of sigma phases is detected in FSP of 316L austenite stainless steel in this study. Although the exact formation mechanism of sigma phases to date is not clear, it is likely attributable to high strain and recrystallization induced by FSP. In general, sigma phase is formed during aging at temperatures between 773 and 1073 K. The direct decomposition of austenite to sigma phase requires long times due to the accompanying redistribution of alloying elements by mutual diffusion [19]. However, sigma formation can be accelerated in the duplex microstructure of ferrite and austenite phases and can be significantly accelerated by strain and recrystallization during aging [21–23]. Since FSW or FSP introduces high strain and it accompanies dynamic recrystallization in the SZ, Park et al. [17] have suggested that the sigma phase can be rapidly formed by the transformation of austenite to delta-ferrite at high temperatures and the subsequent decomposition of the ferrite to sigma phase.

Current experimental results suggest that the heat input has a significant effect on sigma phase precipitation during FSP. The higher the heat input, the larger the amount of sigma phase formation. As we know, high heat input simultaneous means low cooling rate during FSP. In other words, the duration between the critical temperature ranges of sigma phase formation increases with increasing heat input, which certainly will results in more sigma phase precipitation during cooling. From restraining sigma phase formation point of view, low heat input is necessary.

4. Conclusions

In summary, the following conclusions are reached. Firstly, sigma phase precipitation is confirmed by transmission electron microscopy in friction stir processing of 316L austenite stainless steel. Secondly, from the heat input point of view, the amount of sigma phase precipitation has direct ratio relations with heat input in current experimental conditions. The higher the heat input, the larger the amount of sigma phase formation. The formation of sigma phase produces Cr depletion in banded structure, which results in the largely degraded corrosion resistance in this region. Finally, the present study suggests that low heat input (i.e. low rotation speeds, low working loads and high welding speed) contributes to restrain sigma phase precipitation during FSP of 316L stainless steel.

Acknowledgment

The work was funded by the "Innovative Nuclear Research and Development Program" of the Ministry of Education, Culture, Sports, Science and Technology (MEXT), Japan.

References

[1] S. Ishino, J. Nucl. Mater. 233–237 (1996) 1535.
[2] S. Ishino, J. Nucl. Mater. 251 (1997) 225.
[3] W.M. Thomas, E.D. Nicholas, J.C. Needham, M.G. Murch, P. Templesmith, C.J. Dawes, GB Patent Application No. 9125978.8, December 1991.
[4] C.G. Rhodes, M.W. Mahoney, W.M. Bingel, R.A. Spurling, W.H. Bampton, Scripta Mater. 36 (1997) 69.
[5] M.W. Mahoney, C.G. Rhodes, J.G. Flintoff, R.A. Spurling, W.H. Bampton, Metall. Mater. Trans. A 29 (1998) 1955.
[6] Y.S. Sato, H. Kokawa, M. Enomoto, S. Jogan, Metall. Mater. Trans. A 30 (1999) 2429.
[7] Y.S. Sato, H. Kokawa, M. Enomoto, S. Jogan, T. Hashimoto, Metall. Mater. Trans. A 30 (1999) 3125.
[8] K.V. Jata, S.L. Semiatin, Scripta Mater. 43 (2000) 743.
[9] Y.S. Sato, S.H.C. Park, H. Kokawa, Metall. Mater. Trans. A 32 (2001) 3033.
[10] Y.S. Sato, H. Kokawa, Metall. Mater. Trans. A 32 (2001) 3023.
[11] G.M.D. Cantin, S.A. David, W.M. Thomas, E. Lara-Curzio, S.S. Babu, Sci. Technol. Weld. Joining 10 (2005) 268.
[12] S.H.C. Park, Y.S. Sato, H. Kokawa, Scripta Mater. 49 (2003) 161.
[13] D. Zhang, M. Suzuki, K. Maruyama, Scripta Mater. 52 (2005) 899.
[14] A.H. Feng, Z.Y. Ma, Scripta Mater. 56 (2007) 397.
[15] C.I. Chang, C.J. Lee, J.C. Huang, Scripta Mater. 51 (2004) 509.
[16] W. Woo, H. Choo, D.W. Brown, P.K. Liaw, Z. Feng, Scripta Mater. 54 (2006) 1859.
[17] S.H.C. Park, Y.S. Sato, H. Kokawa, K. Okamoto, S. Hirano, M. Inagaki, Scripta Mater. 49 (2003) 1175.
[18] S.H.C. Park, Y.S. Sato, H. Kokawa, K. Okamoto, S. Hirano, M. Inagaki, Scripta Mater. 51 (2004) 101.
[19] M. Schwind, J. Kallqvist, J.O. Nilsson, J. Agren, H.O. Andren, Acta Mater. 48 (2000) 2473.
[20] K. Okamoto, S. Hirano, M. Inagaki, S.H.C. Park, Y.S. Sato, H. Kokawa, in: Proceedings of the 4th International Symposium on Friction Stir Welding, Park City, Utah, 2003 (CD-ROM).
[21] J.M. Vitek, S.A. David, Weld. J. 63 (1984) 246s.
[22] R.A. Farrar, J. Mater. Sci. 20 (1985) 4215.
[23] J.M. Vitek, S.A. David, Weld. J. 65 (1986) 106s.
[24] Y.C. Chen, H. Fujii, T. Tsumura, Y. Kitagawa, K. Nakata, K. Ikeuchi, K. Matsubayashi, Y. Michishita, Y. Fujiya, J. Katoh, Sci. Technol. Weld. Joining 14 (2009) 197.